

# A Miniaturized Dual-Band MIMO Antenna with Low Mutual Coupling for Wireless Applications

Mohssine El Ouahabi<sup>1, \*</sup>, Alia Zakriti<sup>1</sup>, Mohamed Essaadi<sup>2</sup>,  
Aziz Dkiouak<sup>1</sup>, and Hanae Elftouh<sup>3</sup>

**Abstract**—In this article, a parasitic element structure is proposed to reduce the mutual coupling in a miniaturized microstrip dual-band Multiple-Input Multiple-Output (MIMO) antenna, which resonates at (7.8 GHz) for X-band and at (14.2 GHz) for Ku band applications. The design of the primary antenna consists of two identical radiators placed on a  $24 \times 20 \text{ mm}^2$  Fr-4 substrate, which are excited by orthogonal microstrip feed lines. In addition, a single complementary split ring resonator (S-CSR) is used to improve the performance of proposed antenna. Simulation and measurement were used to study the antenna performance, including reflection coefficients, coupling between the two input ports, radiation efficiency, and the radiation pattern. The measured results show that the proposed antenna achieves two operating bands with impedance bandwidths ( $|S_{11}| \leq -10 \text{ dB}$ ) of 560 MHz (7.6 to 8.16 GHz) and 600 MHz (13.8 to 14.4 GHz) and mutual coupling ( $|S_{12}| < -26 \text{ dB}$ ), which are suitable for X/Ku band applications.

## 1. INTRODUCTION

Multiple-Input Multiple Output (MIMO) technology is one of the most dynamic areas of research that offers a significant increase in channel capacity and wireless system efficiency and meets the growing demand for high-speed wireless communication systems [1]. It is characterized by its spatial diversity and multi-path property. However, when antenna elements are placed in a confined space, the space limitation will produce a strong coupling between ports and then degrade the antenna performance such as diversity gain.

In this context, a compact MIMO system with low coupling between collocated antenna elements has become a real challenge for antenna designers, and several decoupling methods have been devoted to this issue. For example, defected ground structures (DGS) [2–4] and metamaterial structures in [5–7] have been applied to achieve high isolation in MIMO antenna systems. Also, the weak mutual coupling between the ports of a two orthogonal patches antenna has been designed in [8] for the 2.4 GHz industrial, science, and medical (ISM) band. However, neutralization-line [9, 10] has been used to improve the isolation between two-monopole-antenna system. There are still other methods to achieve a better isolation by using metalized via wall [11], electromagnetic band-gap (EBG) structure [12–14], etching slots in the ground plane [15, 16], and ELC resonator [17].

In this paper, a compact dual-band MIMO antenna with high isolation is designed using the orthogonal microstrip line. The two frequency bands are obtained by embedding a particular form inside the radiation patch and loading two symmetrical slits in the same patch. However, the performance

---

*Received 26 March 2019, Accepted 22 May 2019, Scheduled 10 June 2019*

\* Corresponding author: Mohssine El Ouahabi (elouahabi87@gmail.com).

<sup>1</sup> Laboratory of Sciences and Advanced Technology, Department of Civil and Industrial Sciences and Technologies, National School of Applied Sciences, Abdelmalek Essaadi University, Tetuan, Morocco. <sup>2</sup> Mohammed V University, ENSIAS, Rabat, Morocco.

<sup>3</sup> Information Systems and Telecommunications Laboratory, Department of Physics, Faculty of Science, Abdelmalek Essaadi University, Tetuan, Morocco.

of proposed antenna is optimized by embedding a single split ring resonator in ground plane. By adjusting the geometrical parameter of each slit in the radiator, both frequency bands can be controlled independently. The low mutual coupling and low envelope correlation coefficient make the proposed antenna a good candidate for MIMO/diversity systems in the entire frequency band.

## 2. ANTENNA GEOMETRY AND DESIGN ASPECTS

### 2.1. The Evolve Process of the Proposed Antenna Design

The procedure to design a dual-band MIMO antenna with high isolation is shown in Figure 1. Initially, Antenna 1 starts with two identical elements placed parallel to each other on a compact space with a

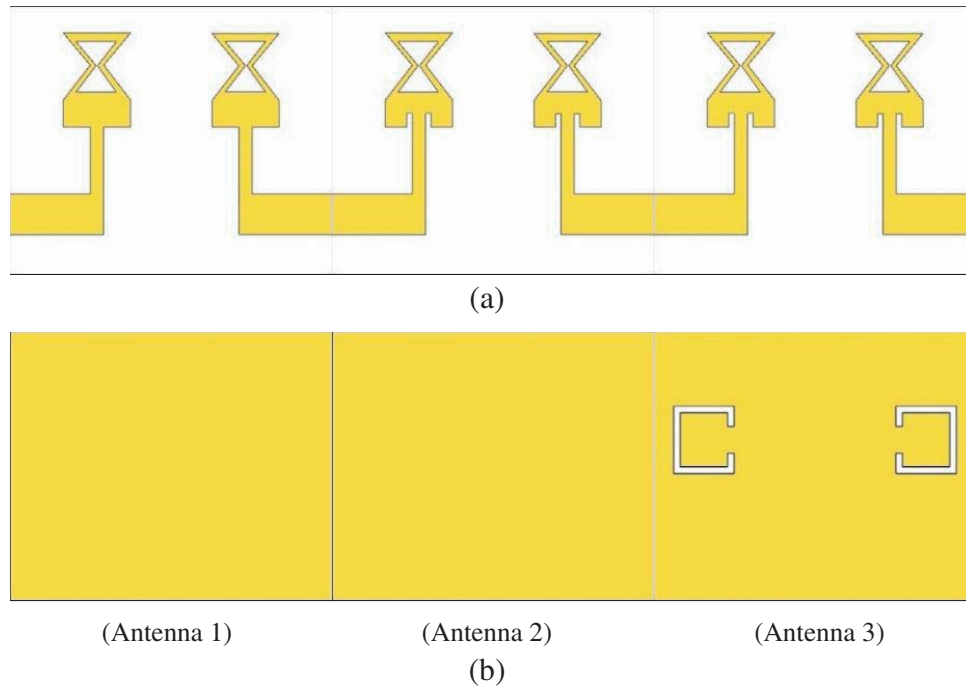


**Figure 1.** Design evolution of proposed MIMO antenna: (a) front view, (b) bottom view.

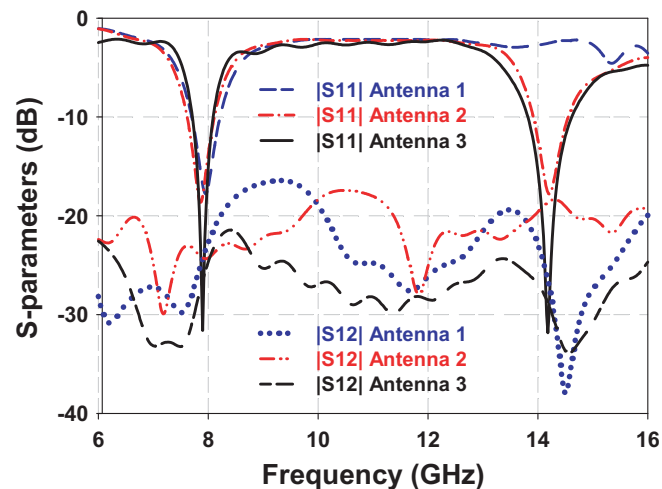


**Figure 2.** Simulated  $S$ -parameters of all structures.

complete ground plane. By embedding a particular form inside the radiation patch, the first frequency band at 7.8 GHz can be achieved as shown in Figure 2. In order to make the antenna resonate at the second frequency band, each radiating element in Antenna 2 is loaded by two symmetrical slits. So, the second resonance frequency is achieved at 14.2 GHz, whereas in Antenna 3, a single split ring resonator is etched in the back substrate side to get a higher impedance matching over the operating dual bands as displayed in the  $|S_{11}|$  plot (Figure 2). The commercial software CST Microwave Studio is used to design and analyze the  $S$ -parameter of each step of the proposed MIMO antenna.

### 2.2. Design of Proposed MIMO Antenna

The final geometry of the proposed dual-band MIMO antenna is illustrated in Figure 3. It is fabricated on a compact FR4 substrate of  $24 \times 20 \text{ mm}^2$  with a relative permittivity of 4.4 and a substrate thickness of 1.6 mm. The optimized geometrical parameters of presented antenna are listed in Table 1.

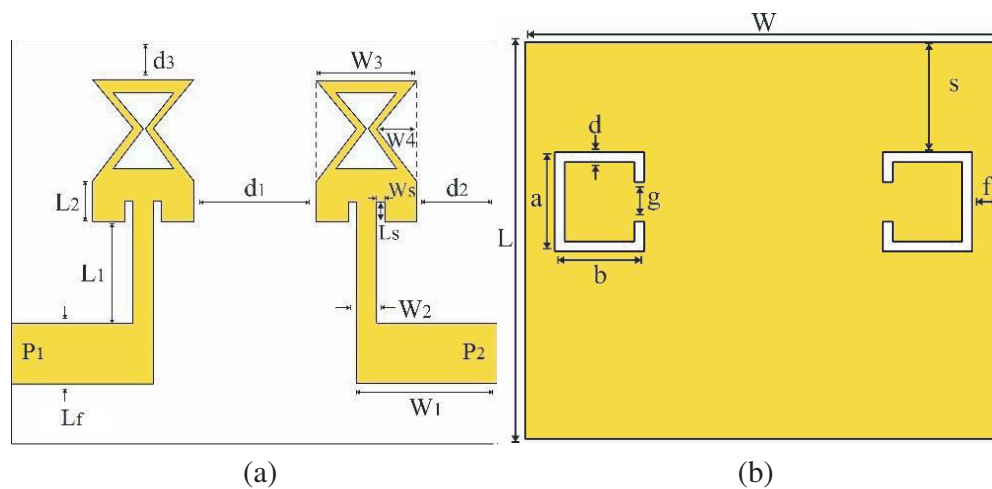


**Figure 3.** The geometry of proposed MIMO antenna: (a) top view, (b) bottom view.

**Table 1.** Dimensions of the proposed antenna.

Parameters	$L$	$W$	$L_f$	$L_1$	$L_2$	$W_1$	$W_2$	$W_3$	$W_4$	$d_1$
Value (mm)	20	24	3	5	2	7	1	5	2	6
Parameters	$d_2$	$d_3$	$a$	$b$	$d$	$g$	$f$	$s$	$L_s$	$W_s$
Value (mm)	4	2	4.5	4.5	0.5	2.5	1.5	7	1	0.4

### 2.3. Study the Effect Lengths of Proposed Antenna

To further evaluate the performance of antenna design, a parametric study is carried out on two geometrical parameters “ $W_4$ ” and “ $L_s$ ”, respectively. These parameters have an important effect on both frequency bands. Figure 4 exhibits the effect of parameter “ $W_4$ ” on return Loss of the proposed antenna. It can be seen that the first frequency band is shifted from 8.2 GHz ( $W_4 = 1.6 \text{ mm}$ ) to 7.6 GHz ( $W_4 = 2.4 \text{ mm}$ ). These descriptions show the effect of  $W_4$  on the first resonant frequency.

The simulated return loss of proposed antenna with different values of “ $L_s$ ” is presented in Figure 5.  $L_s$  corresponds to slots length. It is observed from Figure 5 that by increasing the value of  $L_s$ , the second resonating frequency is also shifted toward the higher frequency.

It can also be observed from Figures 4 and 5 that the isolation between ports is not influenced significantly by different values of “ $W_4$ ” and “ $L_s$ ”. Based on this study, the optimal values of  $W_4$  and  $L_s$  are as follows:  $W_4 = 2 \text{ mm}$  and  $L_s = 1 \text{ mm}$ .

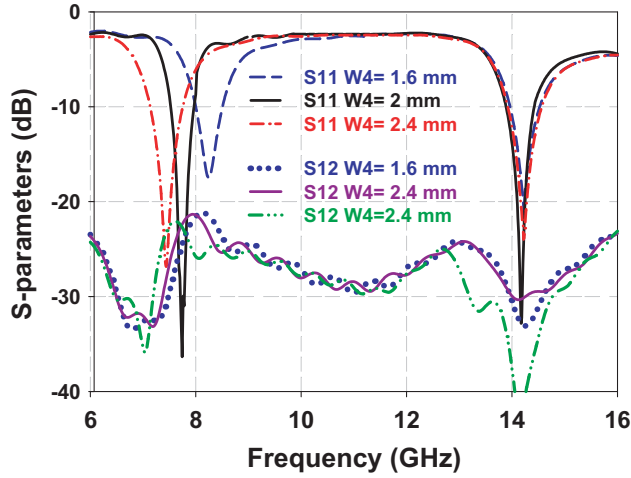


**Figure 4.** Simulated return loss results of proposed antenna with variation of parameter  $W_4$ .

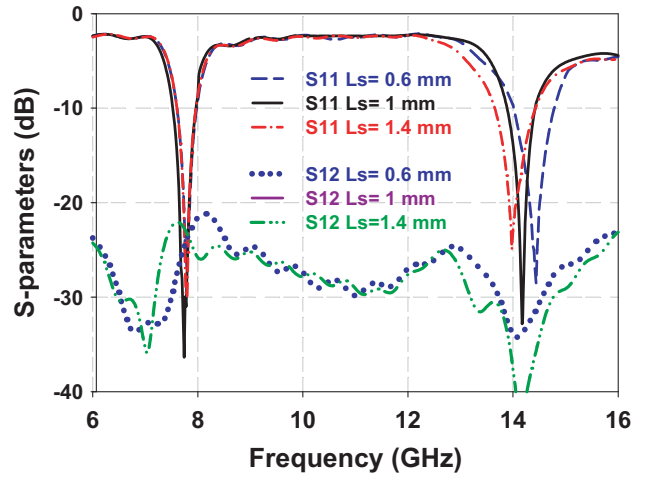


**Figure 5.** Simulated return loss results of proposed antenna with variation of parameter  $L_s$ .

### 3. FABRICATION AND MEASUREMENT RESULTS

#### 3.1. Fabricated Antenna and Measured Results

Based on the optimized dimensions shown in Figure 3, a prototype of the proposed antenna has been successfully fabricated on an FR4 substrate (dielectric constant = 4.4, loss tangent = 0.02) using LPKF ProtoMat E33 compact circuit board plotter device as shown in Figure 6. Then, it is measured experimentally using the A Rohde and Schwarz ZVB 20 vector network analyzer.

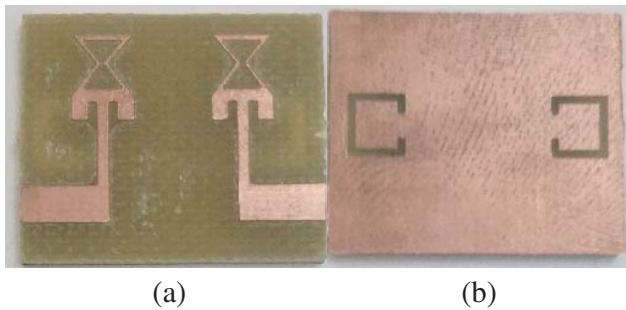


**Figure 6.** Photograph of fabricated prototype antenna: (a) the front view, (b) bottom view.

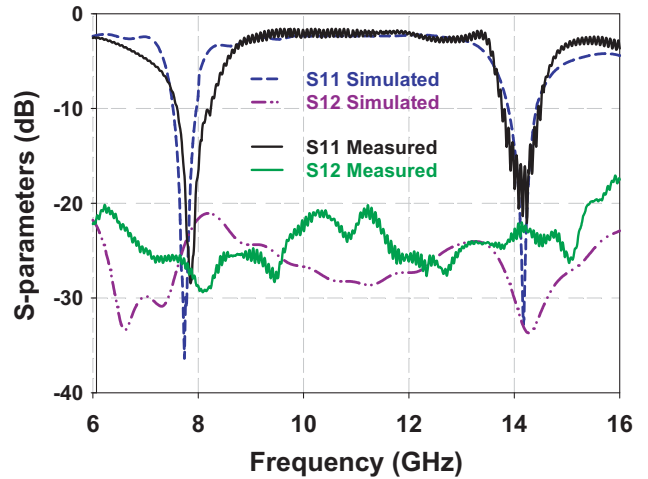


**Figure 7.** Simulated and measured  $S$ -parameters  $|S_{11}|$  and  $|S_{12}|$  versus frequency of the proposed antenna.

Figure 7 shows the comparison between measured and simulated  $S$ -parameters of the proposed antenna. Due to the symmetric structure of the proposed antenna, the simulated and measured  $|S_{22}|$  and  $|S_{21}|$  are almost the same as  $|S_{11}|$  and  $|S_{12}|$ , and they are not shown in this figure for the sake of brevity.

The experimental results are in close agreement with the simulated ones. As can be seen from measured results, the impedance bandwidth ( $|S_{11}| < -10$  dB) of fabricated MIMO antenna can cover

the lower frequency band 7.6–8.16 GHz (X-band) with the maximum value of 28 dB at 7.83 GHz, and in the higher frequency band 13.8–14.4 GHz (Ku-band) with the maximum value of 20 dB at 14.2 GHz. In addition, along the frequency range, the measured isolation values between ports over the operating bands are less than  $-26$  and  $-22$  dB, respectively. This indicates a high isolation for the proposed dual-band MIMO antenna.

### 3.2. Diversity Performance

This section presents an analysis of diversity performance of proposed MIMO antenna in terms of envelope correlation coefficient, diversity gain, and radiation efficiency.

The envelope correlation coefficient is an important metric to study MIMO antenna systems and can be computed using the far-field patterns described in detail in [18]. The correlation coefficient  $ECC(i, j)$ , between the  $i$ th and  $j$ th antenna elements is calculated and put as the following formula:

$$ECC(i, j) = \frac{\left( \oint (X_{PR}E_{\theta i}(\Omega)E_{\theta j}^*(\Omega)P_{\theta}(\Omega) + E_{\varphi i}(\Omega)E_{\varphi j}^*(\Omega)P_{\varphi}(\Omega)) d(\Omega) \right)^2}{\oint (X_{PR}G_{\theta i}(\Omega)P_{\theta}(\Omega) + G_{\varphi i}(\Omega)P_{\varphi}(\Omega)) d(\Omega) \cdot \oint (X_{PR}G_{\theta j}(\Omega)P_{\theta}(\Omega) + G_{\varphi j}(\Omega)P_{\varphi}(\Omega)) d(\Omega)} \quad (1)$$

In the case of uniform multipath environment, Equation (2) can now be expressed as the envelope correlation coefficient ECC for two antenna elements:

$$ECC = \frac{\left( \oint (E_{\theta 1}(\Omega)E_{\theta 2}^*(\Omega) + E_{\varphi 1}(\Omega)E_{\varphi 2}^*(\Omega)) d(\Omega) \right)^2}{\oint (G_{\theta 1}(\Omega) + G_{\varphi 1}(\Omega)) d(\Omega) \cdot \oint (G_{\theta 2}(\Omega) + G_{\varphi 2}(\Omega)) d(\Omega)} \quad (2)$$

where  $E_1$  and  $E_2$  are the far-field radiation patterns, generated from ports 1 and 2, respectively.

The diversity gain (DG) from ECC [19, 20] can be calculated to evaluate the MIMO antenna performance by using Equation (3):

$$DG = 10 \times \sqrt{1 - |\rho|^2} \quad (3)$$

where  $\rho$  is the complex cross correlation coefficient, with

$$|\rho|^2 \approx ECC \quad (4)$$

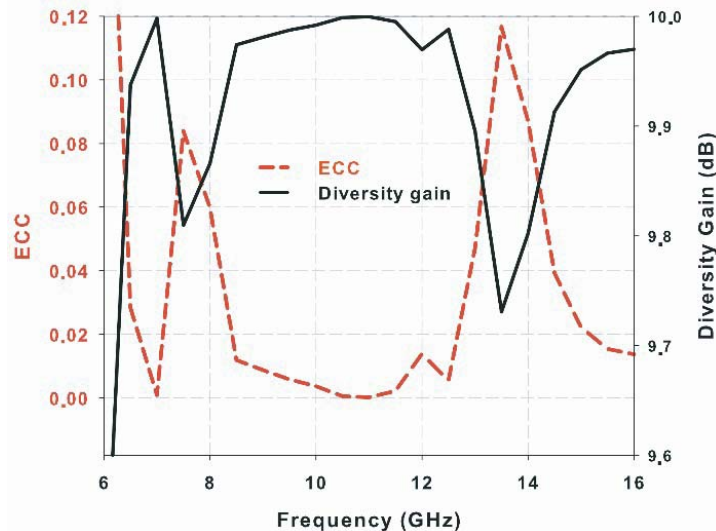
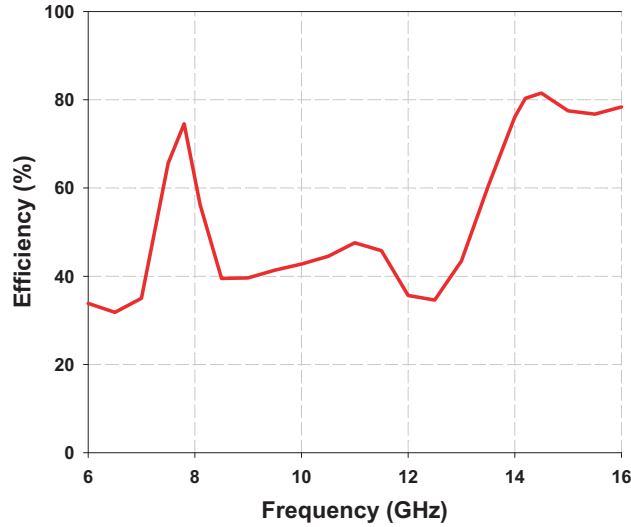


Figure 8. Envelope correlation coefficient and diversity gain of proposed antenna.

Figure 8 shows the correlation coefficient between the antenna elements of the proposed MIMO antenna system from far-field radiation patterns. We can notice that the maximum values of correlation coefficient are 0.07 and 0.04 in the region of resonances and within the acceptable limits. According to the same figure, the diversity gain for both bands is greater than 9.8 dB, which means that the proposed MIMO antenna has a good diversity gain performance.



**Figure 9.** Simulated radiation efficiency of proposed antenna.

Figure 9 shows the simulated radiation efficiency plots of the proposed antenna. The radiation efficiency is around 80% across the operating bands.

### 3.3. Surface Current Distributions

The surface current distributions of presented MIMO antenna at desired frequency bands 7.8 GHz and 14.2 GHz are shown in Figure 10. It can be seen that when port 1 is excited and port 2 terminated with a 50-Ω load, a strong current appears on port 2 around the particular form inside the radiation patch and on the single-CSRR in lower band, whereas for upper band, more surface current is induced in a slit. Thus, both slit and single-CSRR helps to achieve high isolation over the operating dual bands of the proposed MIMO antenna. This effect remains the same when port 2 is excited and port 1 terminated with a 50-Ω load.

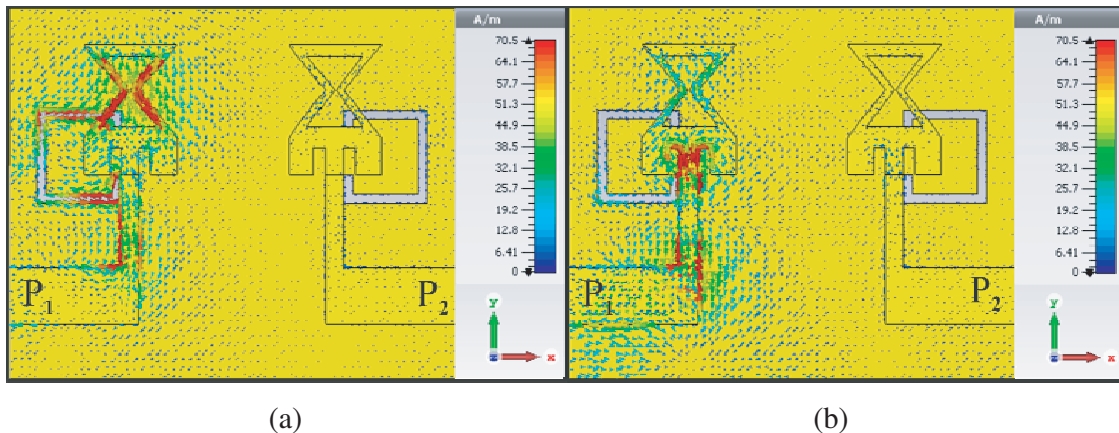


**Figure 10.** Surface current distribution at: (a) 7.2 GHz and (b) 14.2 GHz.

### 3.4. Radiation Patterns

The simulated and measured radiation patterns of the proposed MIMO antenna at the frequencies of 7.8 GHz and 14.2 GHz in the *E*- and *H*-planes when port 1 is excited and port 2 terminated with a 50-Ω load are plotted in Figures 11(a) and (b), respectively. Note that the radiation patterns in the *H*-plane

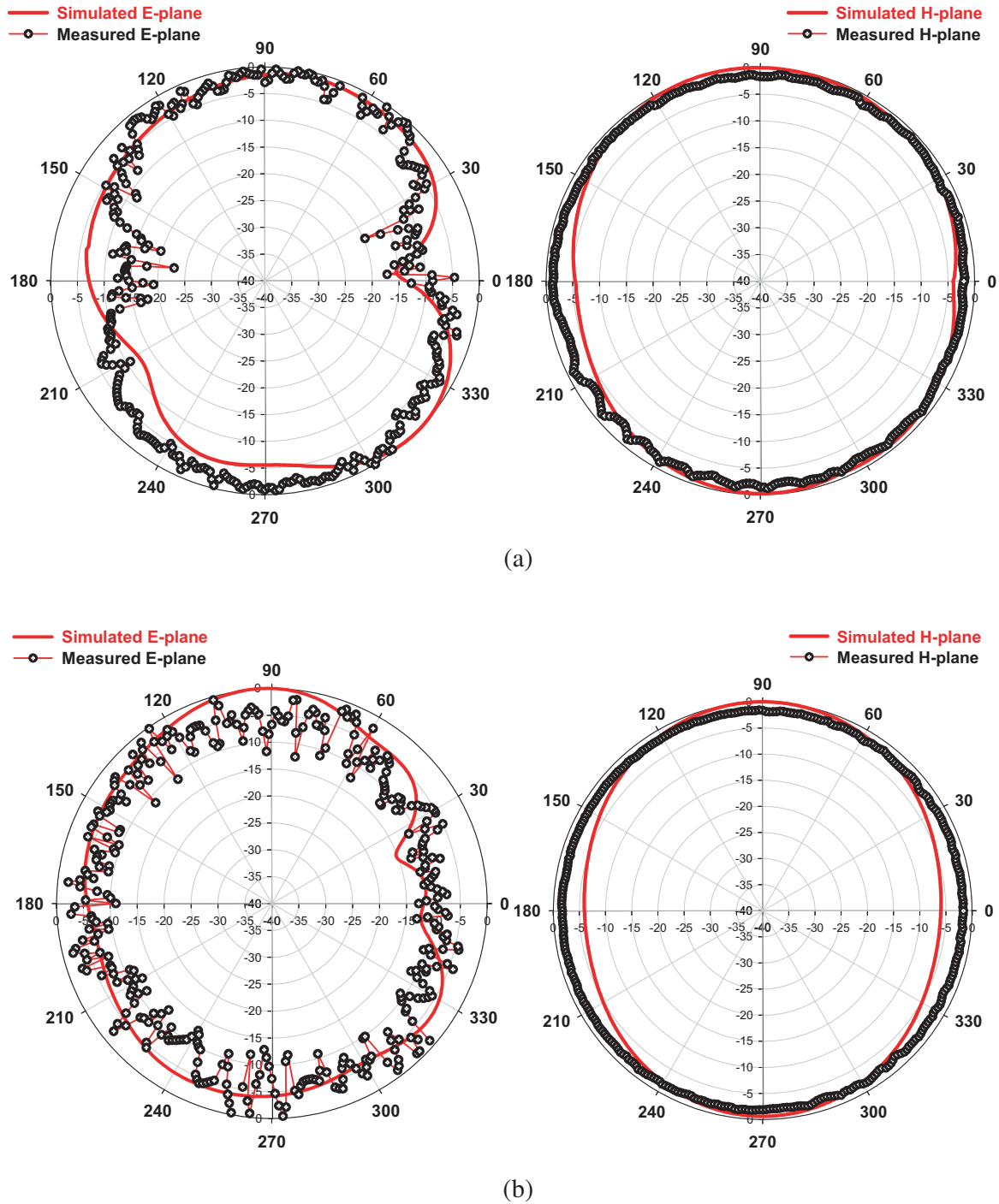


**Figure 11.** Radiation patterns of proposed antenna *E*-plane (left) and *H*-plane (right) at: (a) 7.8 GHz, (b) 14.2 GHz.

is nearly omnidirectional and identical to radiation pattern of dipole antenna in  $E$ -plane, which is quite suitable for X-band and Ku-band applications. We can also notice that there are some ripples in the measured pattern compared with the simulated one due to reflections coming from the condition of measurement and the chamber that was not helicoidal, which reflected waves.

### 3.5. Performance Comparison

The comparisons of the proposed MIMO array among other referenced designs are listed in Table 2. We can show from this table that the proposed antenna has high isolation, low ECC, and small size compared to the reported MIMO antenna.

**Table 2.** Performance comparison among the proposed (PS) antenna and other MIMO antenna.

Ref. No	Antenna Size (mm <sup>3</sup> )	Number of Elements Used	Minimum Isolation (dB)	ECC	Sub.	$\epsilon_r$
P.S	$24 \times 20 \times 1.6$	2	22	$< 0.07$	FR-4	4.4
[21]	$50.54 \times 21.29 \times 1.59$	2	18.43	$< 0.2$	Fr-4	4.4
[22]	$25 \times 25 \times 1.6$	4	15	$< 0.14$	FR-4	4.4
[23]	$17 \times 42 \times 1.6$	2	13	$< 0.015$	FR-4	4.4

## 4. CONCLUSION

A compact dual-band MIMO antenna for X-band and Ku-band applications has been presented in this paper. A parametric study has been carried out to show the effect of various parameters on the performances of the proposed MIMO antenna. Using a single complementary split ring resonator helps to achieve a significant isolation less than  $-22$  dB in two operating bands (X and Ku). The central frequency of each band can be easily adjusted by altering the geometrical parameters of corresponding slit. In addition, the antenna has  $ECC < 0.04$ , diversity gain  $> 9.8$  dB, radiation efficiency around 80%, and stable radiation patterns over the operating bands. Thus, the proposed dual-band MIMO antenna is an appropriate candidate for X-band and Ku-band applications.

## ACKNOWLEDGMENT

This work was partially supported by faculty of sciences, under information systems and telecommunications laboratory, Abdelmalek essaâdi university, Tetuan, Morocco, Supervised by professor Mohsine KHALLADI.

## REFERENCES

1. Shin, H. and J. H. Lee, "Capacity of multiple-antenna fading channels: Spatial fading correlation, double scattering, and keyhole," *IEEE Transactions on Information Theory*, Vol. 49, No. 10, 2636–2647, Oct. 2003.
2. Anitha, R., V. P. Sarin, P. Mohanan, and K. Vasudevan, "Enhanced isolation with defected ground structure in MIMO antenna," *Electronics Letters*, Vol. 50, No. 24, 1784–1786, 2014.
3. Kamal, S. and A. A. Chaudhari, "Printed meander line MIMO antenna integrated with air gap, DGS and RIS: A low mutual coupling design for LTE applications," *Progress In Electromagnetics Research C*, Vol. 71, 149–159, 2017.
4. Habashil, A., J. Nourinia, and C. Ghobadi, "A rectangular defected ground structure (DGS) for reduction of mutual coupling between closely-spaced microstrip antennas," *20th Iranian Conference on Electrical Engineering, (ICEE 2012)*, May 15–17, 2012.

5. Yang, D. G., D. O. Kim, and C.-Y. Kim, "Design of dual-band MIMO monopole antenna with high isolation using slotted CSSRR for WLAN," *Microw. Opt. Technol. Lett.*, Vol. 56, 2252–2257, 2014.
6. Iqbal, A., O. A. Saraereh, A. Bouazizi, and A. Basir, "Metamaterial-based highly isolated MIMO antenna for portable wireless applications," *Electronics*, Vol. 7, No. 10, 267, Oct. 22, 2018.
7. Arora, C., S. S. Pattnaik, and R. N. Baral, "SRR superstrate for gain and bandwidth enhancement of microstrip patch antenna array," *Progress In Electromagnetics Research B*, Vol. 76, 73–85, 2017.
8. Nigam, H. and M. Kumar, "A compact MIMO antenna design for 2.4 GHz ISM band frequency applications," *International Journal of Electronics and Computer Science Engineering*, 324–331, 2014.
9. Kayabasi, A., A. Toktas, E. Yigit, and K. Sabanci, "Triangular quad-port multi-polarized UWB MIMO antenna with enhanced isolation using neutralization ring," *AEU — International Journal of Electronics and Communications*, 2017.
10. Zhang, S. and G. F. Pedersen, "Mutual coupling reduction for UWB MIMO antennas with a wideband neutralization line," *IEEE Antennas and Wireless Propagation Letters*, Vol. 15, 166–169, 2016.
11. K. A. I. D. A. Xu and J. Zhu, "Wideband patch antenna using multiple parasitic patches and its array application with mutual coupling reduction," *IEEE Access*, Vol. 6, 42497–42506, 2018.
12. Jaglan, N., S. D. Gupta, B. K. Kanaujia, S. Srivastava, and E. Thakur, "Triple band notched DG-CEBG structure based UWB MIMO/diversity antenna," *Progress In Electromagnetics Research C*, Vol. 80, 21–37, 2018.
13. Kumar, N. and U. Kiran Kommuri, "MIMO antenna mutual coupling reduction for WLAN using spiro meander line UC-EBG," *Progress In Electromagnetics Research C*, Vol. 80, 65–77, 2018.
14. Dabas, T., D. Gangwar, B. K. Kanaujia, and A. K. Gautam, "Mutual coupling reduction between elements of UWB MIMO antenna using small size uniplanar EBG exhibiting multiple stop bands," *AEU — International Journal of Electronics and Communications*, 2018.
15. Kokkinos, T., E. Liakou, and A. P. Feresidis, "Decoupling antenna elements of PIFA arrays on handheld device," *Electronics Letters*, Vol. 44, No. 25, 1442–1444, 2008.
16. Azarm, B., J. Nourinia, C. Ghobadi, M. Majidzadeh, and N. Hatami, "On development of a MIMO antenna for coupling reduction and WiMAX suppression purposes," *AEU — Int. J. Electron. Commun.*, Vol. 99, 226–235, 2018.
17. Pandit, S., A. Mohan, and P. Ray, "A compact planar MIMO monopole antenna with reduced mutual coupling for WLAN applications using ELC resonator," *Proceedings of the Asia-Pacific Microwave Conference*, 2016.
18. Zhang, J., J. Ou Yang, K. Z. Zhang, and F. Yang, "A novel dual-band MIMO antenna with lower correlation coefficient," *International Journal of Antennas and Propagation*, Vol. 2012, 7 pages, Article ID 512975, 2012.
19. Pierce, J. N. and S. Stein, "Multiple diversity with non-independent fading," *Proceedings of the IRE*, Vol. 48, 89–104, Jan. 1960.
20. Schwartz, M., W. R. Bennett, and S. Stein, *Communication System and Techniques*, 470–474, McGraw-Hill, New York, 1965.
21. Satam, V. and S. Nema, "Defected ground structure planar dual element MIMO antenna for wireless and short range RADAR application," *2015 IEEE Int. Conf. Signal Process. Informatics, Commun. Energy Syst., SPICES 2015*, Feb. 2015.
22. Nirdosh, C. M. Tan, and M. R. Tripathy, "A miniaturized T-shaped MIMO antenna for X-band and Ku-band applications with enhanced radiation efficiency," *27th Wirel. Opt. Commun. Conf. WOCC, 2018*, Vol. 1, 1–5, 2018.
23. Pouyanfar, N., C. Ghobadi, J. Nourinia, K. Pedram, and M. Majidzadeh, "A compact multi-band MIMO antenna with high isolation for C and X bands using defected ground structure," *Radioengineering*, Vol. 27, No. 3, 686–693, 2018.